Chemical Physics Letters 683 (2017) 121–127

Contents lists available at ScienceDirect

Chemical Physics Letters

journal homepage: www.elsevier.com/locate/cplett

Research paper

Femtosecond real-time probing of reactions MMXVII: The predissociation of sodium iodide in the A 0^+ state

Gennady Rasskazov [a], Muath Nairat [a], Ilias Magoulas [a], Vadim V. Lozovoy [a], Piotr Piecuch [a,b,*], Marcos Dantus [a,b,*]

[a] Department of Chemistry, Michigan State University, East Lansing, MI 48824, USA
[b] Department of Physics and Astronomy, Michigan State University, East Lansing, MI 48824, USA

ARTICLE INFO

Article history:
Received 10 January 2017
In final form 7 February 2017
Available online 9 February 2017

ABSTRACT

We revisit the femtosecond transition-state spectroscopy of sodium iodide taking advantage of modern lasers and pulse-shaping to better map the low-lying electronic states, some forming predissociative wells through curve crossings. We also carry out high-level *ab initio* multi-reference configuration interaction calculations including spin-orbit coupling terms and using large correlation-consistent basis sets to arrive at accurate ground- and excited-state potential energy curves of NaI. Density matrix calculations employing vibrational wave functions determined from the *ab initio* X 0^+ and A 0^+ potentials are used to simulate time dependent wave packet dynamics of NaI pumped to the A 0^+ state.

1. Introduction

One of the initial publications on the femtosecond real-time observation of transition states in a chemical reaction [1] demonstrated how femtosecond laser pulses could open a window to explore the spectroscopic transformation of reagents into products. In the case of cyanogen iodide (ICN), dissociation of the I-CN bond occurred directly, but the observation of wave packet oscillations during the dissociation of alkali halides [2] provided a clear example of predissociation, showing that femtosecond pulses could reveal spectroscopic information that was very difficult to obtain by other methods. Among the alkali halides, sodium iodide (NaI) became one of the systems that Zewail explored in detail, returning to it every few years [3–8]. This, in turn, triggered substantial follow-up work further exploring, theoretically as well as experimentally, the dynamics of sodium iodide [9–15]. For all these reasons, we have chosen to revisit one of Zewail's favorite molecular systems, taking advantage of technical and theoretical advances that have taken place in the nearly 30 years since the initial NaI work [2].

Given that the spectroscopy, potential energy curves, and femtosecond dynamics of NaI have already been extensively studied and reviewed in the literature, we immediately proceed to the statement of the main goal of the present study. We have noticed that while a number of frequency- and time-resolved experiments have been aimed at mapping the ground and lower excited states of NaI, there remain large discrepancies in the description of the excited A 0^+ state, especially near the bottom of the A 0^+ well. We have, therefore, decided to carry out a thorough examination of the lower vibrational energy levels in the A 0^+ state and their predissociation dynamics. We analyze both time- and frequency-resolved measurements, including our own and those reported in the literature, and compare them with the results of *ab initio* electronic structure and dynamics calculations.

Our study takes advantage of major advances in laser technology in recent years, for example, the solid-state kilohertz repetition-rate Ti:Sapphire regeneratively amplified femtosecond lasers, which are much more stable than the 20 Hz system used by Zewail's group in 1988, which had 8 different laser dye circulators, with solutions that had to be refreshed on a weekly basis. We also take advantage of a pulse shaper and the multiphoton intrapulse interference phase scan (MIIPS) technique, capable of measuring and compressing the pulses to their transform-limited duration automatically [16–19]. In the case of theoretical analyses and electronic structure calculations, we take advantage of computers that are orders of magnitude faster than in 1988. We also benefit from significant progress in quantum chemistry and the existence of better codes and algorithms compared to 1988. We use, for example, highly efficient version of the *ab initio* multi-reference configuration interaction (MRCI) methodology with the explicit inclusion of spin-orbit (SO) interactions, coupled with large and carefully optimized correlation-consistent basis sets, to arrive at accurate ground- and excited-state potential energy curves

* Corresponding author at: Department of Chemistry, Michigan State University, East Lansing, MI 48824, USA.
E-mail addresses: piecuch@chemistry.msu.edu (P. Piecuch), dantus@msu.edu (M. Dantus).

http://dx.doi.org/10.1016/j.cplett.2017.02.019
0009-2614/

(PECs) of the NaI system, which are subsequently used to determine vibrational term values and wave functions helpful in the examination of the experimental data. All of this allows us to provide the most accurate description of the lower electronic states of NaI, especially the A 0^+ state, to date.

2. Experimental and computational details

The experiments were performed using a regeneratively amplified Ti:Sapphire laser system (Spectra Physics, Spitfire) producing 40 fs pulses at a central wavelength of 798 nm with 0.8 mJ pulse energy at a repetition rate of 1 kHz. The experiments were run using the pump-probe method. The output pulses from the amplifier were split in a Mach-Zehnder interferometer with adjustable optical delay stage and were spatially recombined by a dichroic mirror. The pump pulse with a central wavelength of 399 nm and transform-limited 30 fs pulse duration was prepared from the output of the pulse shaper [20] (MIIPS-HD, Biophotonic Solutions Inc.) followed by a second harmonic generation (SHG) crystal. The probe pulse with a central wavelength of 798 nm and 45 fs pulse duration was derived from a partial reflection of the beam prior to entering the pulse shaper. For all the experiments, the polarization angle between pump and probe pulses was set at magic angle 54.74° in order to avoid contributions from rotational motion dynamics. Sodium iodide was sealed in vacuum inside a quartz cell; the quartz cell was heated in a cylindrical oven to 873 K. The entire oven was insulated by ceramic bricks in order to thermally insulate that region of the optical table and keep the nearby laser system stable. For pump-probe experiments, the pump wavelength was derived from the second harmonic of the Ti:Sapphire laser resulting in 3.107 eV (25,063 cm^{-1}) pulses that reach the A 0^+ state by a single-photon transition. The probe wavelength was the fundamental of the laser at 798 nm, promoting the excited wave packet through a one-photon resonance to states correlating with the Na($\sim 3p^1$; $^2P_{1/2}$ and $^2P_{3/2}$) + I($\sim 5s^25p^5$; $^2P_{3/2}$) dissociation channel corresponding to sodium D lines. Power dependence for the pump and probe transitions is included in the Supporting Information. The pump and probe beams were focused into the cell by a 225 cm focal length lens. The fluorescence of sodium atoms (sodium D line, unresolved doublet near 589.3 nm) was detected as a function of time delay using a compact spectrometer (QE65000, Ocean Optics). Pump and probe laser intensities were attenuated until they had negligible contribution to the detected signal. For long time scans (greater than 5 ps) we used a conventional optical delay line. For short time scans (less than 5 ps) we used the pulse shaper to scan the arrival time of the pump pulse. Power dependence measurements were carried out to ascertain that the signal arises from linear excitation from the ground X 0^+ state to the excited A 0^+ state. For experiments where the pump spectrum was tuned, we took advantage of the pulse shaper to introduce a phase that would cause the SHG spectrum to become sharper and to tune it to different wavelengths because of multiphoton intrapulse interference [16].

The electronic structure calculations of the PECs that correlate with the three lowest-energy dissociation channels of NaI, including Na($\sim 3s^1$; $^2S_{1/2}$) + I($\sim 5s^25p^5$; $^2P_{3/2}$), Na($\sim 3s^1$; $^2S_{1/2}$) + I($\sim 5s^25p^5$; $^2P_{1/2}$), and Na^+($\sim 2s^22p^6$; $^1S_0$) + I^-($5s^25p^6$; $^1S_0$), were performed using the MOLPRO 2010.1 program [21]. We used the internally contracted MRCI approach [22–24] based on the complete active-space self-consistent field (CASSCF) [25,26] reference wave functions resulting from the state-averaged (SA) CASSCF calculations, incorporating SO interactions at the MRCI theory level, as further elaborated on below. The calculations were performed on a dense grid of Na-I distances ranging from 1.6 to 30 Å and the C_{2v} symmetry was employed throughout. For the smaller sodium atom, the augmented polarized valence correlation-consistent aug-cc-pV*n*Z basis sets with n = T, Q, and 5 were employed [27]. For the heavier iodine atom, the inner 28 electrons ([Ar]$3d^{10}$) were replaced by the relativistic effective core potential (ECP) of Peterson et al. [28]; the remaining 25 electrons outside the ECP were described by the corresponding aug-cc-pV*n*Z-PP basis sets, again with n = T, Q, and 5 [28]. Throughout the rest of this work, both families of basis sets are abbreviated AV*n*Z. For the sake of brevity, only the results corresponding to the largest Na and I basis sets, namely AV5Z, are discussed more thoroughly. The complete set of the MRCI/AV*n*Z + SO energies for all computed states and for all basis sets used in this study can be found in the Supporting Information.

The MRCI/AV*n*Z + SO calculations reported in this work were performed in the following three stages. First, we used the SA-CASSCF orbital optimization ignoring SO effects and incorporating all electronic states of NaI that correlate with the two lowest-energy scalar-relativistic (or non-relativistic) dissociation channels, including Na($\sim 3s^1$; ^2S) + I($\sim 5s^25p^5$; ^2P), which gives rise to singlet and triplet states of Σ^+ and Π symmetries (12 states total), and Na^+($\sim 2s^22p^6$; ^1S) + I^-($5s^25p^6$; ^1S), which correlates with the second singlet Σ^+ state. Once the SO interactions are turned on, these two channels correlate with the three lowest-energy SO-coupled dissociation channels mentioned above. In performing our SA-CASSCF calculations, we distributed 8 valence electrons of NaI (the 3s electron of sodium and the 5s and 5p electrons of the iodine atom) among the 8 valence orbitals correlating with the 3s and 3p shells of Na and 5s and 5p shells of I. Next, we performed the internally contracted ECP-based MRCI calculations, still ignoring SO interactions, including single and double excitations from the multi-dimensional reference space that corresponds to the previous CASSCF step, to determine 13 scalar-relativistic states of NaI that correlate with the aforementioned Na($\sim 3s^1$; ^2S) + I($\sim 5s^25p^5$; ^2P) and Na^+($\sim 2s^22p^6$; ^1S) + I^-($5s^25p^6$; ^1S) asymptotes. In doing so, we explicitly correlated 8 valence electrons of NaI. We were unable to correlate more electrons at the MRCI level, since this would require considering additional 18 electrons corresponding to 2s and 2p shells of sodium and the 4d shell of iodine, resulting in prohibitive computer costs. Finally, to account for SO interactions, we diagonalized the $\hat{H}_e + \hat{H}_{SO}$ Hamiltonian, where $\hat{H}_e$ is the ECP-based electronic Hamiltonian and $\hat{H}_{SO}$ stands for the Breit–Pauli operator including SO coupling terms, as implemented in MOLPRO, in the space spanned by the previously determined MRCI/AV*n*Z eigenvectors of $\hat{H}_e$ [29], so that they could be mixed to produce the desired 13 SO-coupled states of NaI that correlate with the three dissociation channels of interest in this work, Na($\sim 3s^1$; $^2S_{1/2}$) + I($\sim 5s^25p^5$; $^2P_{3/2}$), giving rise to the X $0^+ \equiv 0^+$(I), 0^-(I), 1(I), 1(II), and 2 states, Na($\sim 3s^1$; $^2S_{1/2}$) + I($\sim 5s^25p^5$; $^2P_{1/2}$), correlating with the A $0^+ \equiv 0^+$(II), 0^-(II), and 1(III) states, and Na^+($\sim 2s^22p^6$; $^1S_0$) + I^-($5s^25p^6$; $^1S_0$), corresponding to the B $0^+ \equiv 0^+$(III) state. The MRCI/AV*n*Z + SO PECs reported in this work and the energies obtained in the scalar-relativistic ECP-based MRCI calculations prior to the final diagonalization of the $\hat{H}_e + \hat{H}_{SO}$ Hamiltonian in the space spanned by the MRCI/AV*n*Z eigenvectors of $\hat{H}_e$ were not corrected for the quasi-degenerate Davidson corrections. We could not do the former, since the existing MOLPRO's implementation of the MRCI methodology corrected for the SO effects does not allow for the inclusion of the *a posteriori* Davidson corrections (one can do it in the calculations ignoring SO effects, but there is no mechanism to include the Davidson corrections when diagonalizing the $\hat{H}_e + \hat{H}_{SO}$ Hamiltonian in the space spanned by the MRCI/AV*n*Z eigenvectors of $\hat{H}_e$). Furthermore, our attempts to include the quasi-degenerate Davidson corrections in the scalar-relativistic ECP-based MRCI calculations prior to the diagonalization of the $\hat{H}_e + \hat{H}_{SO}$ Hamiltonian produced discontinuities and a non-smooth behavior of the

resulting PECs in the regions of avoided crossings, making such potentials useless in the following computational steps and analysis. The high quality of the final MRCI/AV*n*Z + SO PECs and the resulting vibrational term values show that ignoring the Davidson corrections does not have a substantial effect on our calculations.

In addition to the electronic structure calculations, we determined the vibrational term values of the X 0^+ and A 0^+ states using the MRCI/AV*n*Z + SO PECs by numerically integrating the radial Schrödinger equation for the Na and I nuclei from 1.8 to 20 and from 1.8 to 12 Å for the X 0^+ and A 0^+ states, respectively, using the Numerov–Cooley algorithm [30] found in Le Roy's Level 8.2 program [31]. These vibrational term values can be found in the Supporting Information. In the case of the A 0^+ state, we could not integrate the radial Schrödinger equation beyond 12 Å, since, as discussed later in this work, the A 0^+ state forms a narrow avoided crossing with the B 0^+ state around 11 Å; the proper treatment of vibrations penetrating this region would require performing vibronic calculations coupling the A 0^+ and B 0^+ manifolds. In fact, treating the X 0^+ and A 0^+ states as isolated electronic states for vibrational analyses involving high-energy vibrations in the former state and low-energy vibrations in the latter state is an approximation too, since the X 0^+ and A 0^+ potentials form an avoided crossing around 7 Å, which would require vibronic calculations coupling the X 0^+ and A 0^+ manifolds. Such a coupling would likely reduce the vibrational spacings corresponding to the low-lying vibrational states (to be precise, resonances) in the A 0^+ state compared to the vibrational spacings obtained in this work by treating the A 0^+ well as an isolated potential. We will revisit these issues in the future work.

3. Results

Excitation at 399 nm (3.107 eV) and probing at 798 nm (1.554 eV) would have been inconceivable 20 years ago given that the bottom of the A 0^+ state was thought to be near 3.15 eV [7]. Furthermore, probing required a resonance with a state correlating with excited state sodium (Na*), approximately 2 eV in excitation energy. Nevertheless, such a transient is shown in Fig. 1 with time-delay steps between pump and probe of 50 fs. We observe oscillations with a mean vibrational period of 907 fs, corresponding to 36.77 cm^{-1} vibrational spacing. The oscillatory motion decays with a biexponential having lifetimes of 3.7 ± 0.3 ps ($\alpha = 0.45$) and 21.2 ± 1.3 ps ($\alpha = 0.55$). Fast Fourier-transform (FFT) and maximum entropy method (MEM) analysis of the oscillations leads to the determination of the mean vibrational frequency of 1.1025 THz.

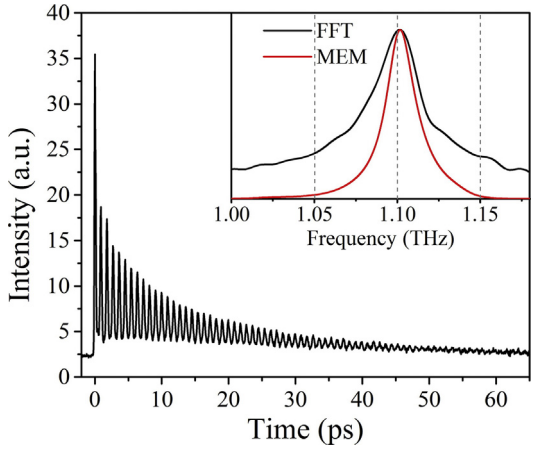

Fig. 1. Experimental FTS transient obtained with 399 nm pump and 798 nm probe laser wavelengths. The inset shows FFT and MEM analysis of the time-resolved transient showing the average vibrational state contributions.

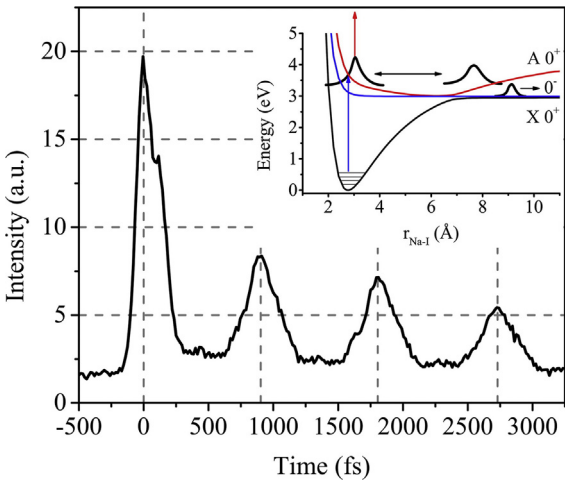

Fig. 2. High resolution experimental FTS transient obtained with 399 nm pump and 798 nm probe laser wavelengths. In this case the probe laser was delayed by the pulse shaper in 15 fs steps. The inset shows the schematic of the relevant MRCI/AV5Z + SO potential energy curves contributing to the signal being detected. From this transient it is clear that probing takes place near the inner turning point of the A 0^+ potential.

High temporal resolution experimental data, shown in Fig. 2, were obtained by using the pulse shaper to generate the time delay between pump and probe pulses. The shaper allows us to generate arbitrary time steps that can be as small as 10 attoseconds. In this case, we scanned the probe pulse with a step size of 15 fs. The scan was carried out up to the first ~3 ps. From this scan, we confirm that the oscillation period of the wave packet is ~908 fs and we further observe that the timing is consistent going back to time zero, when pump and probe pulses are overlapped. We take this fact to confirm that probing with 798 nm pulses takes place near the inner turning point of the wave packet, very close to the Franck-Condon (FC) region where excitation takes place. Furthermore, analysis of the intensity of the time-zero feature indicates that approximately 56% of the excited molecules reach the A 0^+ state while the remaining 44% reach the 0^-(I) and the 2 electronic states correlating with Na(~$3s^1$; $^2S_{1/2}$) + I(~$5s^25p^5$; $^2P_{3/2}$). A power dependence study on the probe wavelength indicates the possibility for 1 + 1 resonant two-photon transition to the repulsive state correlating with dissociation to produce excited state sodium (see the Supporting Information).

The predissociation time for NaI has been one of the key dynamics measured. At the energy of excitation in this study probing the lower-energy part of the A 0^+ potential, the rate of escape from the A 0^+ state is expected to be significantly slower than that found by Zewail using 311 nm pulses. Here we explore within a limited range the wavelength dependence of the escape rate. We used two different wavelengths of excitation, 395 nm (blue) and 402 nm (red) pump wavelengths, while the 798 nm probe laser wavelength and bandwidth were unchanged. Frequency tuning was achieved by introducing a sinusoidal function using the pulse shaper and this resulted in the modified spectrum [16]. Results from those measurements with different excitation spectra are shown in Fig. 3. The energy difference between the two pulses corresponds to 471 cm^{-1}. Biexponential fitting to the data finds a lifetime for the blue excitation of 2.2 ± 0.3 ps ($\alpha = 0.45$) and 18.1 ± 1.1 ps ($\alpha = 0.55$), while for the red wavelength the corresponding constants were 2.7 ± 0.5 ps ($\alpha = 0.45$) and 20.0 ± 1.8 ps ($\alpha = 0.55$). The difference in the predissociation rate amounts to 13%. FFT and MEM analysis show that the mean vibrational

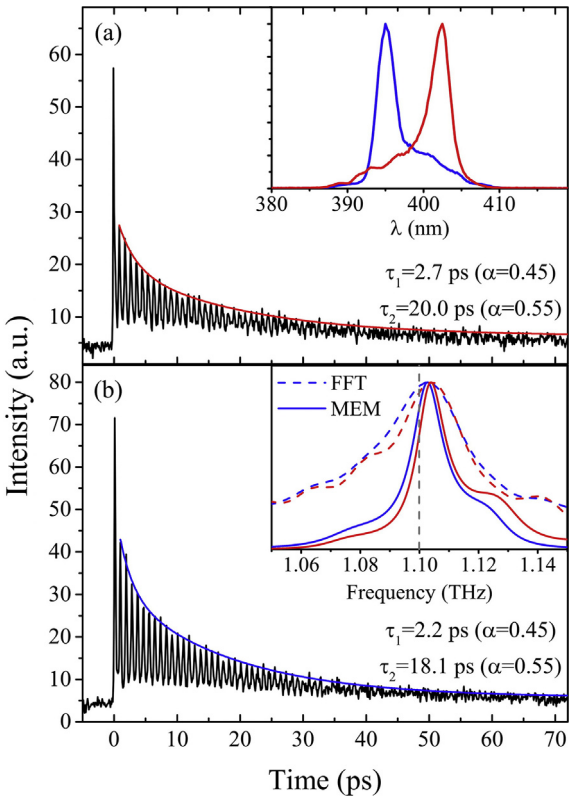

Fig. 3. Experimental FTS transient obtained with (a) 402 nm (red spectrum in the inset of (a)) and (b) 395 nm (blue spectrum in the inset of (a)) pump wavelengths and 798 nm probe laser wavelengths with exponential fitting. The inset of (b) shows the FFT (dashed) and MEM (solid) from the 402 nm (red) and the 395 nm (blue) pump wavelength. (For interpretation of the references to colour in this figure legend, the reader is referred to the web version of this article.)

frequency that is associated with the blue pump is 1.102 THz whereas that with the red pump is slightly larger with a value of 1.104 THz.

The MRCI/AV5Z + SO PECs originating from the three lowest dissociation channels of interest in this work, namely, Na($\sim$3s^1; ^{2}S$_{1/2}$) + I($\sim$5s^{2}5p^5; ^{2}P$_{3/2}$), giving rise to the X 0$^+$, 0$^-$(I), 1(I), 1(II), and 2 states, Na($\sim$3s^1; ^{2}S$_{1/2}$) + I($\sim$5s^{2}5p^5; ^{2}P$_{1/2}$), correlating with the A 0$^+$, 0$^-$(II), and 1(III) states, and Na$^+$($\sim$2s^{2}2p^6; ^{1}S$_0$) + I$^-$(5s^{2}5p^6; ^{1}S$_0$), resulting in the B 0$^+$ state, are depicted in Fig. 4 (see the

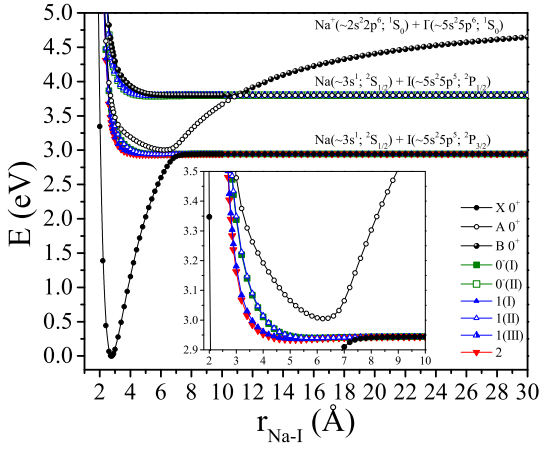

Fig. 4. Potential energy curves of NaI obtained in the MRCI/AV5Z + SO calculations. The inset shows the zoomed in region of the lower-energy avoided crossing.

Supporting Information for the corresponding AVTZ and AVQZ figures). The asymptotic behavior of the potential energy curves reveals the great performance of our high-level *ab initio* calculations. The predicted value of the SO splitting of the iodine atom, read from the MRCI/AV5Z + SO PECs correlating with the lowest two dissociation channels at the Na-I distance r_{Na-I} of 30 Å (the largest distance considered in our calculations), is 0.856 eV, while the experimental one is 0.943 eV [32]. At r_{Na-I} = 30 Å, the energy separation between the ground-state and ionic channels resulting from the MRCI/AV5Z + SO calculations is 1.703 eV. If one assumes a Coulomb attractive potential at very large Na-I distances, the interaction energy between the Na$^+$ and I$^-$ ions at 30 Å is 0.480 eV. Therefore, the theoretically computed dissociation limit characterizing the ionic Na$^+$($\sim$2s^{2}2p^6; ^{1}S$_0$) + I$^-$(5s^{2}5p^6; ^{1}S$_0$) channel resulting from our MRCI/AV5Z + SO calculations is expected to lie 2.183 eV above the ground-state Na($\sim$3s^1; ^{2}S$_{1/2}$) + I($\sim$5s^{2}5p^5; ^{2}P$_{3/2}$) asymptote, in excellent agreement with the difference between the ionization potential of Na (5.139 eV) and the electron affinity of I (3.059 eV) [33]. The high quality of the MRCI/AV5Z + SO PECs is further attested by the calculated spectroscopic constants of the X 0$^+$ state. For the dissociation energy D_0, equilibrium bond length r_e, and harmonic vibrational frequency ω_e, we obtained 2.929 eV, 2.761 Å, and 250.6 cm^{-1}, respectively. The corresponding experimental values are 3.00 eV, 2.711 Å, and 258 cm^{-1} [34]. Furthermore, the energy separation between the X 0$^+$ and A 0$^+$ states reaches a minimum of 0.153 eV at a distance of 6.8 Å, in good agreement with the previously reported values (see Ref. [11] and references therein). Since the employed basis set, namely AV5Z, is close to the complete basis set limit, the scalar-relativistic effects of the heavy iodine atom have already been accounted for through the use of a relativistic ECP, and our calculations include the SO interactions, the observed small deviations from the experimental values are likely due to the facts that MRCI is not an exact theory and core-valence correlations could not be considered at the MRCI level due to their enormous computer costs beyond our present computational capabilities.

As this work focuses on the predissociation of NaI in the A 0$^+$ state, which is populated by transitions from the X 0$^+$ state, and since the X 0$^+$, A 0$^+$, and B 0$^+$ states interact via a series of avoided crossings of the corresponding PECs, resulting in the interesting topology shown in Fig. 4 and the related significant changes in the binding character, we would like to add a few comments about the three lowest-energy $\Omega = 0^+$ states resulting from our MRCI/AV*n*Z + SO calculations. We examined their composition in terms of the MRCI wave functions calculated without the SO coupling, which we could further analyze using the corresponding one-electron reduced density matrices. At the largest Na-I distance considered in our calculations of 30 Å, the X 0$^+$ state is a mixture of the lowest $^1\Sigma^+$ (66.6%) and $^3\Pi$ (33.4%) states in a scalar-relativistic (or non-relativistic) description, which both have a covalent character in that region, with the A 0$^+$ state being the orthogonal (also covalent) complement to the X 0$^+$ state (by covalent, we mean the state characterized by electron sharing at shorter internuclear distances and dissociating into neutral atoms). This should be contrasted by the B 0$^+$ state, which at r_{Na-I} = 30 Å is of purely ionic nature dominated by the second state of the $^1\Sigma^+$ symmetry in a scalar-relativistic description. The situation dramatically changes when we look at the nature of the X 0$^+$ state at its equilibrium geometry of about 2.7 Å, where the X 0$^+$ state is of almost purely X $^1\Sigma^+$ and ionic character. In fact, the X 0$^+$ state remains predominantly ionic up to the avoided crossing with the A 0$^+$ state around 7 Å, becoming covalent (in the above sense) only after that avoided crossing. At the equilibrium geometry of the ground state, the A 0$^+$ state is a mixture of contributions from the $^3\Pi$ state (68.6%) and the second state of $^1\Sigma^+$ symmetry (31.3%), both being covalent in that region, in agreement with the findings of Ref. [11]. As the Na-I bond is

stretched, the percentage of the second state of $^1\Sigma^+$ symmetry increases with a concomitant decrease of the $^3\Pi$ contribution. For example, the A 0^+ state has a much larger contribution from the second state of $^1\Sigma^+$ symmetry (63.9%) and a much smaller contribution from the lowest $^3\Pi$ state (30.8%), when the equilibrium geometry of the A 0^+ state, which is about 6.3 Å, is considered. In the region of the equilibrium geometry of the A 0^+ state and, in general, in the region prior to the avoided crossing of the X 0^+ and A 0^+ states, the A 0^+ state remains covalent, but the character of the A 0^+ state dramatically changes to ionic when the region between the two avoided crossings shown in Fig. 4 is considered. The A 0^+ and B 0^+ states exchange their character at the avoided crossing around 11 Å, with A 0^+ becoming covalent dominated by the $^3\Pi$ state and B 0^+ becoming ionic, dominated by the second $^1\Sigma^+$ state. The avoided crossing between the X 0^+ and A 0^+ states at about 7 Å causes the latter state to form a very wide potential energy well, which spans nearly 9 Å, with a minimum around 6.3 Å. From an experimental point of view, it is useful to point out the large difference between the equilibrium bond lengths characterizing the X 0^+ and A 0^+ states, which is approximately 3.5 Å. For such a large difference between the respective r_e values, we can anticipate that the lowest vibrational levels of the A 0^+ state are not accessible from the lowest vibrational levels of the X 0^+ state (*vide infra*).

The rather peculiar shape of the A 0^+ PEC shown in Fig. 4 is also reflected in the energy differences of successive vibrational levels, $\Delta G_{v'+1/2} = G(v'+1) - G(v')$, resulting from our calculations using the MRCI/AV5Z + SO PEC. The $\Delta G_{v'+1/2}$ values, instead of decreasing monotonically, initially increase from 39.8 cm^{-1} for $v' = 0$ to 41.8 cm^{-1} for $v' = 15$. Afterwards, they decrease until a plateau is reached in the $v' = 58–80$ region, with an average spacing of 39.0 cm^{-1}, and then they decrease again to 27.9 cm^{-1} for the last calculated, $v' = 168$, vibrational level (see the Supporting Information). Interestingly, the unusual shape of the A 0^+ potential seen in this study was predicted in 1991 by Professor L. Pauling. At a private gathering at Caltech, attended by Professors R. Marcus, R. B. Bernstein, and A. H. Zewail, and one of the senior authors of this work (M.D.), Professor Pauling argued that the A 0^+ adiabatic well has to be shaped by the nearby crossing of ionic and covalent states in a diabatic representation (avoided crossing of the adiabatic X 0^+ and A 0^+ PECs), resulting in a particle-in-a-box-like potential near the bottom of the A 0^+ well changing to harmonic and then to a Morse-like potential at higher energies. Ignoring the fact that the A 0^+ state forms another avoided crossing with the B 0^+ state, our MRCI/AV*n*Z + SO calculations and experiments largely confirm this prediction. It is also worth noting that our MRCI/AV*n*Z + SO calculations and experiments support the A 0^+ PEC shape proposed by Linder et al. [36], which is much different than that suggested by Wang et al. [9].

In addition to the vibrational energies, we also calculated the corresponding vibrational wave functions. From these, we calculated FC factors and, using a density matrix formalism, simulated the nuclear wave packet dynamics in the A 0^+ state (see the Supporting Information for a detailed description). As anticipated, we have found that the large difference in r_e values characterizing the X 0^+ and A 0^+ PECs is so large that the FC factors for the excitations from the lower v'' states in the X 0^+ state to the lower v' states in the A 0^+ state are extremely small. We multiplied the calculated FC factors from theory and used a Boltzmann distribution of the v'' states, taking into account that the experiment was conducted at 873 K, and found out that, on average, the majority of the excitations take place from $v'' = 8–10$ to $v' = 70–90$. By computing the aforementioned density matrix, we determined the effective wave packet dynamics in the A 0^+ state and its evolution, which are shown in Fig. 5. The related formal and computational details can be found in the Supporting Information.

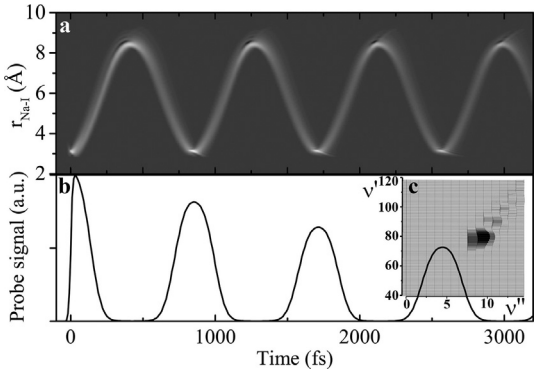

Fig. 5. (a) Calculated wave packet dynamics using the density matrix formalism described in the text. Limited wave packet dephasing is observed given the low anharmonicity of the vibrational levels reached. (b) Pump-probe simulation of the wave packet dynamics with an additional exponential decay. (c) FC and Boltzmann population weighted transition probabilities between the ground and excited states given transform-limited pulses as used for obtaining experimental data in Figs. 1 and 2.

4. Discussion

The NaI system and its predissociation have been studied in great depth for many years, especially after Berry published the initial PECs [35]. Zewail's work [2–8] provided the first observation of quantum beats during the predissociation and showed that by tuning the energy of the pump one could map the relevant PECs. It was observed that for pump energies above 3.6 eV the oscillation period increased, indicating very large anharmonicity associated with the outer turning point of the Coulomb potential. Below 3.6 eV, the period was found to be wavelength independent. The shape of the A 0^+ state below 3.8 eV remained a mystery despite several time- and frequency-resolved spectroscopy measurements and *ab initio* calculations.

Our collaborative work reported in this article combines technical and theoretical advances to provide important new information about the lower excited states of the NaI system, especially the A 0^+ state. We have begun by combining the information about the FC factors involving vibrational wave functions determined from our best *ab initio* X 0^+ and A 0^+ potentials obtained in the MRCI/AV5Z + SO calculations, accounting for the Boltzmann distribution of the vibrational states in the X 0^+ state at the experimental temperature, and the spectrum of the pump pulse. We have found that at the experimental temperature of 873 K the FC factors corresponding to the vibronic X 0^+ (v'') → A 0^+(v') transitions with low values of v'' and v' are so small that such transitions can safely be neglected. Significant excitations occur only when v'' is 8–10. In this case, the maximum transition probabilities involve $v' = 70–90$ levels. According to our calculations, the wave packet is formed at the internuclear distance of about 3 Å, having an excess energy above the bottom of the A 0^+ well of about 3,200 cm^{-1}. Our calculations clearly indicate that the very large difference in r_e values characterizing the X 0^+ and A 0^+ potentials makes the $v' = 0–60$ vibrational states inaccessible by a single photon excitation. Future experimental work, combined with appropriate theoretical analysis, will use multi-pulse excitations to populate lower vibrational levels in the A 0^+ state and to probe their curve crossing dynamics. Our findings regarding vibrational levels in the A 0^+ state accessible in the experiment reported in this work are consistent with the photoabsorption cross sections calculated by Alekseyev et al. [11]. Our findings are also relevant to the work of Tiemann and co-workers, who thoroughly examined the bottom of the A 0^+ well [36]. In Tiemann et al.'s work, results from different experiments and calculations were critically evaluated to

arrive at the A 0^+ potential that is very similar to the one calculated here, in the overall shape and various detailed characteristics. For example, the r_e value characterizing the A 0^+ state determined by Tiemann et al. of 6.052 Å is in very good agreement with our MRCI/AV5Z + SO calculations, which give 6.260 Å.

As far as the observed vibrational periods are concerned, we can compare our *ab initio* findings with Zewail's data [4,7] and our own experimental measurements. This is done in Fig. 6, which displays the observed and calculated wave packet frequencies as functions of the pump wavelength. The calculated wave packet frequencies are defined as the $\Delta G_{v'+1/2}$ values expressed in THz, whereas the pump wavelengths are defined as $G(v') - G(v'' = 0)$ expressed in nm. As we can see, our MRCI/AV5Z + SO calculations, combined with the information about the FC factors and vibrational population according to a Boltzmann distribution of the v'' states at the experimental temperature, provide very good agreement with the experimental findings. It is quite clear that for wavelengths longer than 380 nm one should expect an almost constant wave packet oscillation frequency. This is what we see in our calculations and measurements. The sharp decrease in the wave packet oscillation frequency predicted by our MRCI/AV5Z + SO PECs will be re-examined in the future once we extend our vibrational calculations, which treat the X 0^+ and A 0^+ PECs here as isolated non-interacting potentials, to a vibronic case involving larger ranges of internuclear separations and probing vibrational states/resonances encompassing both avoided crossings seen in Fig. 4 involving the X 0^+, A 0^+, and B 0^+ PECs.

Photopredissociation lifetime analysis was carried by Zewail at 311 nm, with a lifetime of ~4 ps. Based on our MRCI/AV5Z + SO calculations, both A 0^+ and B 0^+ states contribute to the predissociation events at 311 nm. Furthermore, the wave packet dephasing and rephasing may play a role here that needs to be taken into account [37]. We have reviewed Zewail's data in one of his later publications [37] and estimated a biexponential decay to be 2 ± 0.5 ps and 9 ± 1 ps. Our data indicate a biexponential behavior as well, with the first component being about 2.5 ps and the second one of about 19 ps. Note that in our measurements we ignore the first peak when both pump and probe pulses are overlapped because of the significant contribution of the dissociative $0^-(I)$ and 2 states. Given that the excess energy of the wave packet excited at 311 nm is about a factor of two greater than the excess energy of the wave packet excited at 399 nm used in our experiments, the factor of two slower escape found at 399 nm is consistent with the escape probability being proportional to the kinetic energy of the wave packet as it passes near the avoided crossing involving the X 0^+ and A 0^+ states.

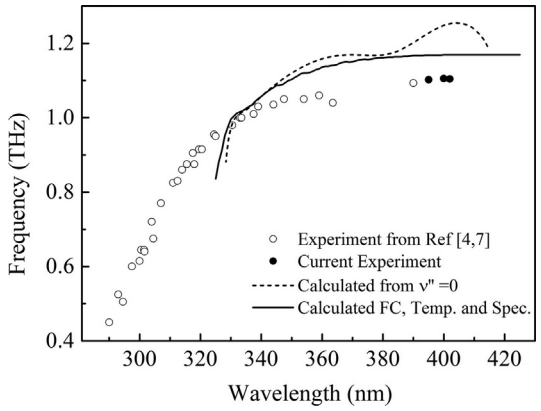

Fig. 6. Vibrational frequency comparison between experiment, Refs. [4,7] and this work, and our calculations. Note that the $v' = 0$–60 vibrational levels in the A 0^+ state are not accessible by a single pulse-pump excitation because of their very low FC factors. We have not carried out the calculations for the excitation wavelengths shorter than 330 nm because of the B 0^+ state involvement.

To the best of our knowledge, the MRCI/AV5Z + SO calculations reported in this work are the largest and most accurate electronic structure calculations for NaI performed to date. In particular, they are in very good agreement with the most reliable previously published experimental and theoretical studies of the elusive A 0^+ state. As already mentioned, our calculated equilibrium distance characterizing the A 0^+ state, r_e = 6.260 Å, compares favorably with that obtained by Tiemann and co-workers, who estimated it at 6.052 Å [36]. Furthermore, the adiabatic excitation energy from X 0^+ to A 0^+ resulting from our MRCI/AV5Z + SO calculations, T_e = 24,240 cm^{-1}, is in good agreement with the value determined by Tiemann et al., T_e = 25,207 cm^{-1} [36]. The avoided crossing between the X 0^+ and A 0^+ states resulting from our best MRCI/AV5Z + SO calculations occurs at ~6.8 Å, in good agreement with the previously reported information as well, while the energy gap between the two states at this distance is only somewhat larger than the values reported in Ref. [11] and references therein. It is interesting to note that independent of the basis set used in our MRCI + SO calculations, the A 0^+ state has approximately the same number of vibrational levels below its Na($\sim 3s^1$; $^2S_{1/2}$) + I($\sim 5s^2 5p^5$; $^2P_{1/2}$) asymptote as the X 0^+ state below the Na($\sim 3s^1$; $^2S_{1/2}$) + I ($\sim 5s^2 5p^5$; $^2P_{3/2}$) asymptote, even though the depth of the A 0^+ potential well measured in this way is approximately one third of the ground-state one. This observation can be rationalized by the unusually large width of the A 0^+ well, which results in much smaller energy spacings between adjacent vibrational levels when compared to the vibrations in the X 0^+ state (see the Supporting Information for the details). As already pointed out, the vibrational levels in the X 0^+ and A 0^+ states were obtained here by treating each PEC as an isolated potential. In reality, the A 0^+ state experiences two avoided crossings, one at a larger distance of about 11 Å with the B 0^+ state and another one near its equilibrium geometry with the X 0^+ state (at about 7 Å). This means that our vibrational levels in the A 0^+ state, especially the low-lying ones, which formally are resonances, have spacings that are possibly somewhat larger compared to what they really ought to be due to the presence of the avoided crossing with the X 0^+ state that enables wave packet escape and predissociation. We plan to examine this issue further by incorporating vibronic couplings in our future calculations.

Finally, our density matrix dynamics wave packet simulations based on our best MRCI/AV5Z + SO potentials, taking into account information about the spectra of pump pulses employed in our experiments and thermal population of the initial vibrational states in the X 0^+ state, were carried out to simulate the observed wave packet dynamics in the A 0^+ state. We have found that the wave packet evolution is very harmonic, which agrees with the fact that we are exciting a very harmonic region of the A 0^+ potential (see Fig. 5). This leads to reduced wave packet dephasing and the possible role it could play in determining the escape of the wave packet from the well. Our dynamics calculations are in very good agreement with experiment. The period obtained in our wave packet dynamics simulations based on the *ab initio* potentials calculated in this work is ~850 fs (see Fig. 5). This is only about 6% faster than the period found experimentally (see, e.g., Fig. 2). While this small difference can be attributed to the numerical precision of the calculations reported in this work, we believe that one of the main reasons for the observed discrepancy is the aforementioned strong interaction between the X 0^+ and A 0^+ states near the avoided crossing, which may translate into effective broadening of the A 0^+ potential well, allowing the penetration of a wider range of Na-I distances by the wave packet during oscillations i.e., longer periods, while increasing the rates of escape. The relatively large rotational temperature of the NaI molecules after excitation may

play a role here too. When we calculated the expected oscillation frequency given the most probable rotational energy level ($J = 52$), we have obtained slightly longer periods, although still ~5% faster than what is measured experimentally.

In addition to being a retrospective look at the NaI system in this commemorative issue, we are also looking toward the future. In this work, we used programmable femtosecond pulses to obtain high-quality time-resolved data, which were then used to guide theoretical calculations in the sense of determining what level of theory is required to reach reasonable agreement with experiment. One of the important extensions of the work reported in this paper will be to probe the pump wavelength region where the B 0^+ state contributes to the wave packet dynamics as well. This will allow us to explore multi-pulse strategies to reach the bottom of the A 0^+ well.

Acknowledgements

This work was supported by the Chemical Sciences, Geosciences and Biosciences Division, Office of Basic Energy Sciences, Office of Science, U.S. Department of Energy (Grant Nos. DE-SC0002325, experimental work aimed at understanding and controlling molecular dynamics in the gas phase, M.D., and DE-FG02-01ER15228, P.P.) and the National Science Foundation (Grant No. CHE-1464807, molecular dynamics calculations and development of novel spectroscopic methods, M.D.).

Appendix A. Supplementary material

Supplementary data associated with this article can be found, in the online version, at http://dx.doi.org/10.1016/j.cplett.2017.02.019.

References

[1] M. Dantus, M.J. Rosker, A.H. Zewail, J. Chem. Phys. 87 (1987) 2395.
[2] T.S. Rose, M.J. Rosker, A.H. Zewail, J. Chem. Phys. 88 (1988) 6672.
[3] V. Engel, H. Metiu, R. Almeida, R.A. Marcus, A.H. Zewail, Chem. Phys. Lett. 152 (1988) 1.
[4] T.S. Rose, M.J. Rosker, A.H. Zewail, J. Chem. Phys. 91 (1989) 7415.
[5] A. Materny, J.L. Herek, P. Cong, A.H. Zewail, J. Phys. Chem. 98 (1994) 3352.
[6] J.L. Herek, A. Materny, A.H. Zewail, Chem. Phys. Lett. 228 (1994) 15.
[7] P. Cong, G. Roberts, J.L. Herek, A. Mohktari, A.H. Zewail, J. Phys. Chem. 100 (1996) 7832.
[8] K.B. Møller, N.E. Henriksen, A.H. Zewail, J. Chem. Phys. 113 (2000) 10477.
[9] J. Wang, A.J. Blake, D.G. McCoy, L. Torop, Chem. Phys. Lett. 175 (1990) 225.
[10] C. Meier, V. Engel, J.S. Briggs, J. Chem. Phys. 95 (1991) 7337.
[11] A.B. Alekseyev, H.-P. Liebermann, R.J. Buenker, N. Balakrishnan, H.R. Sadeghpour, S.T. Cornett, M.J. Cavagnero, J. Chem. Phys. 113 (2000) 1514.
[12] W. Kim, W. Qin, D.G. McCoy, L.W. Torop, Chem. Phys. 264 (2001) 401.
[13] C. Kumar Modal, S.P. Bhattacharyya, Int. J. Quant. Chem. 88 (2002) 310.
[14] D.M. Koch, Q.K. Timerghazin, G.H. Peslherbe, B.M. Ladanyi, J.T. Hynes, J. Phys. Chem. A 110 (2006) 1438.
[15] Q.K. Timerghazin, D.M. Koch, G.H. Peslherbe, J. Chem. Phys. 124 (2006) 034313.
[16] K.A. Walowicz, I. Pastirk, V.V. Lozovoy, M. Dantus, J. Phys. Chem. A 106 (2002) 9369.
[17] V.V. Lozovoy, I. Pastirk, K.A. Walowicz, M. Dantus, J. Chem. Phys. 118 (2003) 3187.
[18] V.V. Lozovoy, I. Pastirk, M. Dantus, Opt. Lett. 29 (2004) 775.
[19] B. Xu, J.M. Gunn, J.M.D. Cruz, V.V. Lozovoy, M. Dantus, J. Opt. Soc. Am. B 23 (2006) 750.
[20] Y. Coello, V.V. Lozovoy, T.C. Gunaratne, B. Xu, I. Borukhovich, C.-H. Tseng, T. Weinacht, M. Dantus, J. Opt. Soc. Am. B 25 (2008) A140.
[21] H.-J. Werner, P.J. Knowles, G. Knizia, F.R. Manby, M. Schütz, P. Celani, T. Korona, R. Lindh, A. Mitrushenkov, G. Rauhut, K.R. Shamasundar, T.B. Adler, R.D. Amos, A. Bernhardsson, A. Berning, D.L. Cooper, M.J.O. Deegan, A.J. Dobbyn, F. Eckert, E. Goll, C. Hampel, A. Hesselmann, G. Hetzer, T. Hrenar, G. Jansen, C. Köppl, Y. Liu, A.W. Lloyd, R.A. Mata, A.J. May, S.J. McNicholas, W. Meyer, M.E. Mura, A. Nicklass, D.P. O'Neill, P. Palmieri, K. Pflüger, R. Pitzer, M. Reiher, T. Shiozaki, H. Stoll, A.J. Stone, R. Tarroni, T. Thorsteinsson, M. Wang, MOLPRO, Version 2010.1, a Package of *Ab Initio* Programs, see <http://www.molpro.net>.
[22] H.-J. Werner, P.J. Knowles, J. Chem. Phys. 89 (1988) 5803.
[23] P.J. Knowles, H.-J. Werner, Chem. Phys. Lett. 145 (1988) 514.
[24] P.J. Knowles, H.-J. Werner, Theor. Chim. Acta 84 (1992) 95.
[25] K. Ruedenberg, M.W. Schmidt, M.M. Gilbert, S.T. Elbert, Chem. Phys. 71 (1982) 41.
[26] B.O. Roos, Adv. Chem. Phys. 69 (1987) 399.
[27] B.P. Prascher, D.E. Woon, K.A. Peterson, T.H. Dunning, A.K. Wilson, Theor. Chem. Acc. 128 (2011) 69.
[28] K.A. Peterson, B.C. Shepler, D. Figgen, H. Stoll, J. Phys. Chem. A 110 (2006) 13877.
[29] A. Berning, M. Schweizer, H.-J. Werner, P.J. Knowles, P. Palmieri, Mol. Phys. 98 (2000) 1823.
[30] J.W. Cooley, Math. Comp. 15 (1961) 363.
[31] R.J. Le Roy, J. Quant. Spectrosc. Radiat. Transfer 186 (2017) 167.
[32] Y.R.A. Kramida, J. Reader, NIST Atomic Spectra Database (Ver. 5.3), 2015.
[33] CRC Handbook of Chemistry and Physics, 2015–2016.
[34] K.P. Huber, G. Herzberg, Molecular Spectra and Molecular Structure, Constants of Diatomic Molecules, vol. 4, Van Nostrand Reinhold, Princeton, NJ, 1979.
[35] R.S. Berry, J. Chem. Phys. 27 (1957) 1288.
[36] J. Lindner, H. Bluhm, A. Fleisch, E. Tiemann, Can. J. Phys. 72 (1994) 1137.
[37] A.H. Zewail, Faraday Discuss. 91 (1991) 207.